Systematics of $B(E2;0_1^+ \rightarrow 2_1^+)$ values for even-even nuclei

S. Raman and C. W. Nestor, Jr.
Oak Ridge National Laboratory, Oak Ridge, Tennessee 37831

K. H. Bhatt*
Western Kentucky University, Bowling Green, Kentucky 42101
(Received 25 September 1987)

We have completed a compilation of experimental results for the electric quadrupole transition probability $B(E2)\uparrow$ between the 0^+ ground state and the first 2^+ state in even-even nuclei. The adopted $B(E2)\uparrow$ values have been employed to test the various systematic, empirical, and theoretical relationships proposed by several authors (Grodzins, Bohr and Mottelson, Wang *et al.*, Ross and Bhaduri, Patnaik *et al.*, Hamamoto, Casten, Möller and Nix, and Kumar) on a global, local, or regional basis. These systematics offer methods for making reasonable predictions of unmeasured $B(E2)$ values. For nuclei away from closed shells, the SU(3) limit of the intermediate boson approximation implies that the $B(E2)\uparrow$ values are proportional to $(e_pN_p+e_nN_n)^2$, where e_p (e_n) is the proton (neutron) effective charge and N_p (N_n) refers to the number of valence protons (neutrons). This proportionality is consistent with the observed behavior of $B(E2)\uparrow$ vs N_pN_n. For deformed nuclei and the actinides, the $B(E2)\uparrow$ values calculated in a schematic single-particle "SU(3)" simulation or large single-j simulation of major shells successfully reproduce not only the empirical variation of the $B(E2)\uparrow$ values but also the observed saturation of these values when plotted against N_pN_n.

I. INTRODUCTION

We have recently completed an exhaustive compilation[1] of experimental results for the reduced electric quadrupole ($E2$) transition probability $B(E2)\uparrow$ between the 0^+ ground state and the first 2^+ state in even-even nuclei. This compilation contains adopted $B(E2)$ values for 281 nuclei. It also contains adopted energies E of the first 2^+ states for these nuclei, together with energies, but not $B(E2)$ values, for an additional 176 nuclei. An overall view of the data in this compilation is shown graphically in Fig. 1. The 2^+ energies are relatively high for nuclei with closed proton or neutron shells and relatively low in the middle of the shells. They also show an overall decrease going from the lightest to the heaviest nuclei. By contrast, the $B(E2)$ values are small for nuclei at the beginning or near the end of a closed shell and attain maximum values for nuclei in the middle of a shell. While the $B(E2)$ values are only about 10 times the single-particle value for nuclei in the 10–40 mass number range, they increase to about 300 times the corresponding value for the transuranium nuclei. These overall trends can be seen in Fig. 1 or in the more detailed figures presented in Ref. 1.

With this $B(E2)$ compilation as a starting point, it is now possible to test[2] the various systematic, empirical, and theoretical relationships that have been proposed by different authors[3–9] to exist amongst these $B(E2)$ values. These systematics constitute the main topic of this paper. They are interesting not only for the intrinsic reason of providing new physics insights but also for the practical reason of supplying a reasonable prediction for a nucleus without an experimentally determined $B(E2)$ value. Even though most of these relationships were proposed one or two decades ago, their use (and subsequent citation) either as a prelude or as a postlude to new measurements has been extremely limited. The absence of an up-to-date comprehensive $B(E2)$ compilation capable of subjecting these relationships to rigorous tests probably contributed to their underutilization.

After presenting in Sec. II some useful formulas relating $B(E2)$ values to mean lifetimes τ or deformation parameters β_2 or intrinsic quadrupole moments Q_0, we proceed to discuss three broad types of systematics in terms of the measured $B(E2)$ values or these related quantities. The first is global systematics which essentially bring out the energy and mass number dependences of the γ-ray transition probability as discussed in Sec. III. Next is local systematics, which bring out the correlations between the $B(E2)$ value for an (N,Z) anchor nucleus and those for the nearby $(N+2,Z)$, $(N,Z+2)$, and $(N+2,Z+2)$ nuclei. This approach is discussed in Sec. IV. The third broad type might be called regional systematics, the regions being bracketed by the magic numbers of protons and neutrons. Five different regions are considered in Sec. V. We attempt in Sec. VI to understand these regional systematics in terms of macroscopic intermediate boson approximation (IBA) and microscopic schematic models. There also exist two global calculations of equilibrium nuclear shapes. The calculation by Möller and Nix[10,11] is based on a macroscopic-microscopic model and that by Kumar[12] on a microscopic model. In Sec. VII, we compare the intrinsic quadrupole moments [which are proportional to the square root of the corresponding $B(E2)$ values] measured for 272 nuclei with those calculated by Möller and

Nix. Though important, this is only a small test because the Möller-Nix calculations extend to about 4000 nuclei. We also compare the measured $B(E2)$ values for 55 nuclei with those calculated by Kumar[12] and his collaborators. Finally, some of our conclusions are discussed in Sec. VIII.

II. USEFUL FORMULAS

We let E denote the energy of the first excited 2^+ state. The basic quantity quoted throughout this paper is the reduced electric quadrupole transition probability $B(E2)\uparrow$ for this state. The mean lifetime of this state [in units of psec if E is in keV and $B(E2)\uparrow$ in e^2b^2] is given by

$$\tau=40.82\times10^{13}E^{-5}[B(E2)\uparrow/e^2b^2]^{-1}(1+\alpha)^{-1} , \quad (1)$$

where α is the total conversion coefficient. The $B(E2)\uparrow$ and τ values are basic experimental quantities. A quantity that, though model dependent, is quite useful because of its easy visualization, is the deformation parameter β_2. Assuming a uniform charge distribution out to the distance $R(\theta,\phi)$ and zero charge beyond, β_2 is related to $B(E2)\uparrow$ by the formula

$$\beta_2=(4\pi/3ZR_0^2)[B(E2)\uparrow/e^2]^{1/2} , \quad (2)$$

where $R_0=r_0A^{1/3}$ is usually taken to be $1.2A^{1/3}$ fm and $B(E2)\uparrow$ is in units of e^2b^2. As an indication of the presence of collective effects in nuclei, the ratio $\beta_2/\beta_{2(\text{s.p.})}$ is quite useful. The quantity $\beta_{2(\text{s.p.})}$ is assumed to be $1.59/Z$, which follows from substituting the Weisskopf single-particle $B(E2)\uparrow$ value into Eq. (2). The intrinsic electric quadrupole moment Q_0 (in units of b) is given by

$$Q_0=\left[\frac{16\pi}{5}\frac{B(E2)\uparrow}{e^2}\right]^{1/2} . \quad (3)$$

The above formulas and other related formulas are also discussed in Ref. 1.

For future use, we also give the hydrodynamic estimates[13] for the $B(E2)\uparrow$ value. For the vibrational mode,

$$B(E2)\uparrow=\frac{45\hbar^2e^2r_0^4}{32\pi^2}\frac{Z^2A^{4/3}}{EB_2} , \quad (4)$$

where B_2 is the inertial mass parameter. For the rotational mode,

$$B(E2)\uparrow=\frac{9\hbar^2e^2r_0^4}{16\pi^2}\frac{Z^2A^{4/3}}{EB_2} . \quad (5)$$

In both cases, the $B(E2)\uparrow$ value varies inversely as the energy E of the first 2^+ state.

III. GLOBAL SYSTEMATICS

A. Systematics of Grodzins

In 1962, Grodzins[3] examined the dependence of the γ-ray transition probability T_γ on the energy of the $2_1^+\rightarrow0_1^+$ transition. He found that 80% of the 126 transition probabilities known at that time were described by the relation (T_γ in psec^{-1} and E in keV)

$$T_\gamma=\tau_\gamma^{-1}=(3\pm1)\times10^{-14}E^4Z^2A^{-1} , \quad (6)$$

which is equivalent to (τ_γ in psec)

$$\tau_\gamma=\tau(1+\alpha)=(3.3\pm1.1)\times10^{13}E^{-4}Z^{-2}A^1 . \quad (7)$$

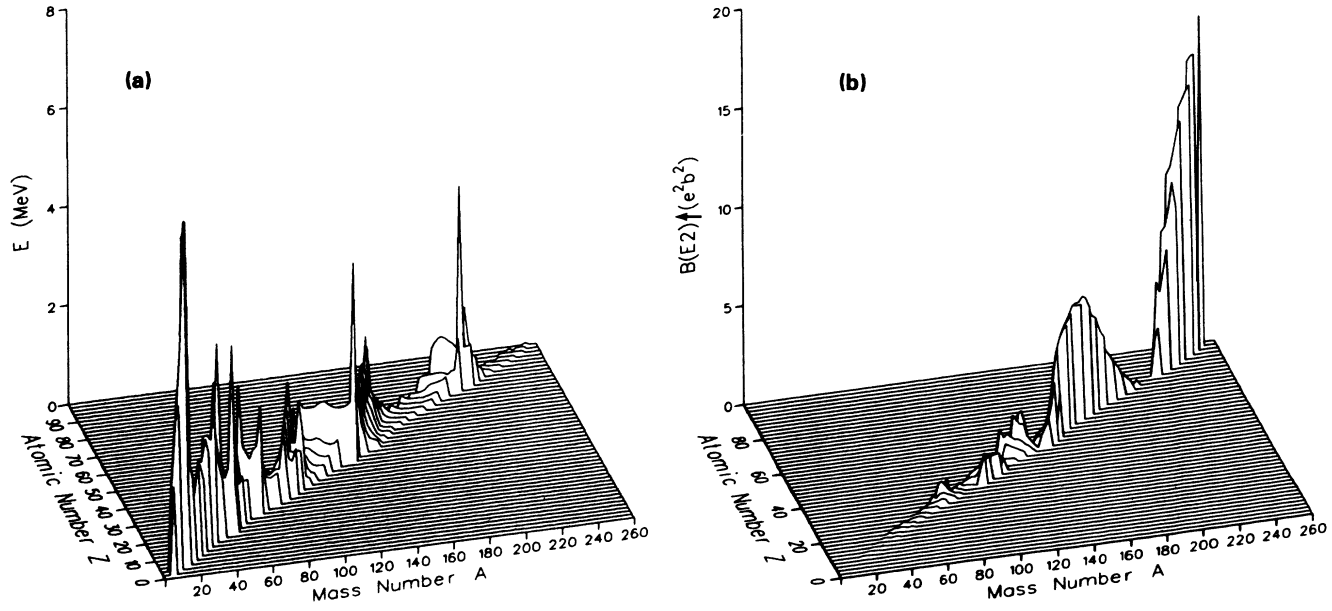

FIG. 1. (a) Energies E of the first excited 2^+ states in even-even nuclei and (b) their corresponding reduced electric quadrupole transition probability $B(E2)\uparrow$ values. This figure is based on the adopted values of Ref. 1.

Following the method chosen by Grodzins to present the data, we show in Fig. 2 a plot of all available τ_γ values versus energy (E) of the first 2^+ states for even-even nuclei. If the exponent of E is fixed as -4, a least-squares fit to the data excluding those for closed-shell nuclei results in (τ_γ in psec)

$$\tau_\gamma = 3.16 \times 10^{12} E^{-4} . \quad (8)$$

This fit is shown by the dashed line in Fig. 2 and has physical significance as discussed below. Permitting the exponent of E to vary results in the following best fit:

$$\tau_\gamma = 4.84 \times 10^{10} E^{-3.4} . \quad (9)$$

This fit is shown by the solid line in Fig. 2.

Reverting to the functional form given in Eq. (7), a least-squares fit to all available τ_γ values except those for closed-shell nuclei results in

$$\tau_\gamma = 2.74 \times 10^{13} E^{-4} Z^{-2} A^{1} . \quad (10)$$

We show in Fig. 3(a) the ratios of calculated [via Eq. (10)] to experimental τ_γ values. Eighty-six percent of these ratios fall between 0.5 and 2.0. The calculated τ_γ values tend to be low [calculated $B(E2)$ values tend to be high] for light nuclei and for nuclei near closed shells.

B. Systematics of Bohr and Mottelson

Within the framework of the hydrodynamic model with irrotational flow, Bohr and Mottelson[4,13] have derived simple expressions for the $B(E2)$ values (and hence for τ_γ values). For small harmonic vibrations of spherical nuclei,

$$\tau_\gamma \approx 0.6 \times 10^{14} E^{-4} Z^{-2} A^{1/3} , \quad (11)$$

and for collective rotations of axially symmetric nuclei,

$$\tau_\gamma \approx 1.4 \times 10^{14} E^{-4} Z^{-2} A^{1/3} . \quad (12)$$

These expressions follow by substituting Eqs. (4) and (5) into Eq. (1). The $E^{-4}Z^{-2}$ dependence in the above expressions was adopted by Grodzins [see Eq. (7)], but he replaced $A^{1/3}$ with A. We find that the experimental data (excluding those for closed-shell nuclei) can be fitted equally well with

$$\tau_\gamma = 5.94 \times 10^{14} E^{-4} Z^{-2} A^{1/3} , \quad (13)$$

which differs from the Bohr and Mottelson expressions [Eqs. (11) and (12)] only in the multiplicative constant. The test of Eq. (13) is shown in Fig. 3(b). Eighty-six percent (the same as for Grodzins) of the calculated:experimental ratios fall between 0.5 and 2.0.

C. Systematics of Wang *et al.*

Another theoretical expression concerning the energy dependence of the $E2$ transition probabilities for the $2_1^+ \rightarrow 0_1^+$ transitions in even-even nuclei was derived by Wang *et al.*[5]. Their expression is (τ_γ in psec and E in keV)

$$\tau_\gamma = 4 \times 10^{8} E^{-3} Z^{-2} A^{2} . \quad (14)$$

Wang *et al.* claimed that they derived the above expression from first principles and without any free parameters. They also claimed that the ratios of values calculated with Eq. (14) to experimental values fell between

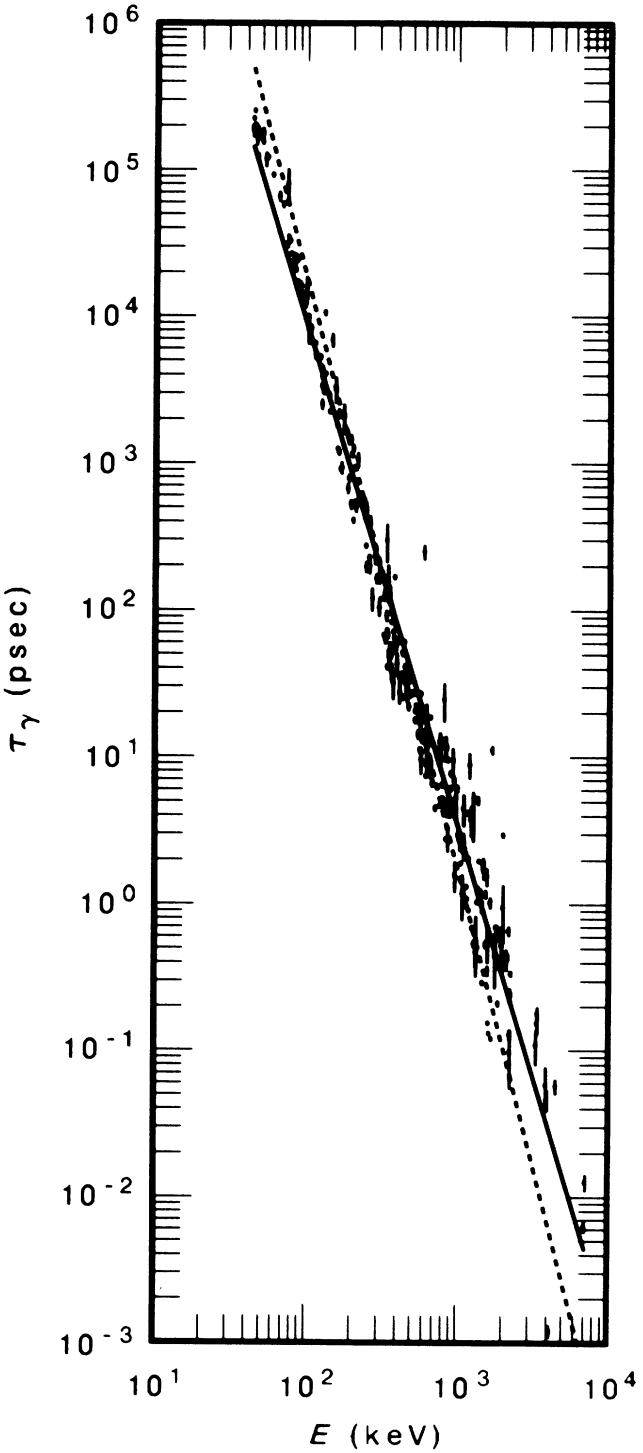

FIG. 2. Gamma-ray mean lifetimes τ_γ as a function of the energies E of the first-excited 2^+ states in even-even nuclei. This plot is similar to Fig. 2 of Grodzins (Ref. 3). The dashed line represents a forced E^{-4} fit to the data and the solid line a best $E^{-3.4}$ fit to the data. In both cases, the data for closed-shell nuclei were omitted in the fits but are included in the plot.

0.2 and 1.7 for 95% of the 214 lifetimes known to them.

We find that the good agreement found by Wang *et al.* is spurious because these authors failed to properly take into account the correction due to internal conversion. Nevertheless, if we retain the functional form of Eq. (14) and carry out a least-squares fit (excluding data for closed-shell nuclei), we obtain

$$\tau_\gamma = 5.25 \times 10^8 E^{-3} Z^{-2} A^2 . \quad (15)$$

The validity of this expression is shown in Fig. 3(c). Fifty-eight percent of the calculated:experimental ratios fall within 0.5 and 2.0. The agreement with the data is inferior to the other two fits [see Figs. 3(a) and (b)].

The work of Wang *et al.* can be faulted for an even more serious reason. Their derivation of Eq. (14) is based on the assumption that the first 2^+ state corresponds to the vibrational excitation of the center of mass of the nucleus. According to Newton's law of motion, the interactions between the nucleons cannot lead to any center-of-mass motion. Hence, despite some apparent success, Eq. (15) has no physical basis.

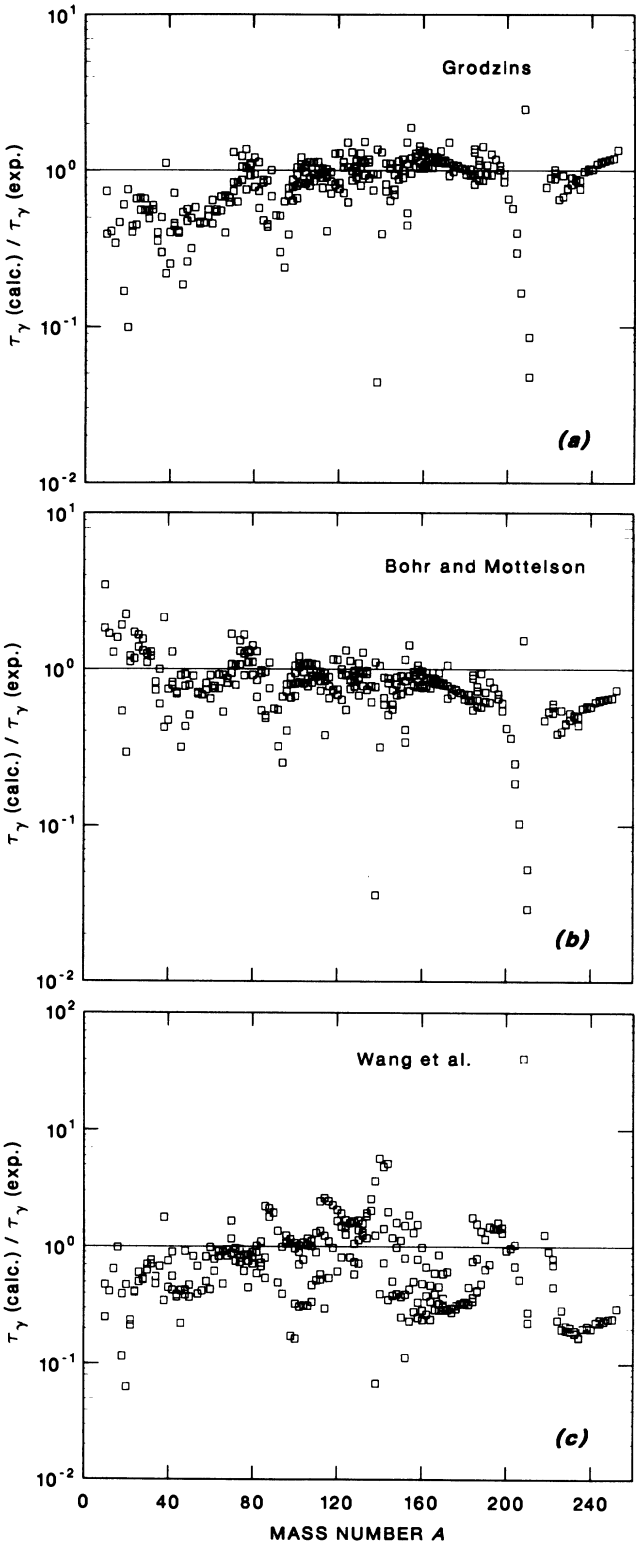

FIG. 3. Ratios of calculated to experimental values of the γ-ray mean lifetimes as a function of the mass numbers. The calculated values correspond to (a) Eq. (10), (b) Eq. (13), and (c) Eq. (15). The experimental values are from Ref. 1.

D. Best global fit

Because the electromagnetic interaction is proportional to Z, the transition probability should vary as Z^2 and hence, the γ-ray mean lifetime as Z^{-2}. With only this constraint, a purely numerical best fit to the data (excluding as before data for closed-shell nuclei), where the exponents of E and A are allowed to vary, yields (τ_γ in psec and E in keV)

$$\tau_\gamma = 1.25 \times 10^{14} E^{-4.0} Z^{-2} A^{0.69} . \quad (16)$$

Figure 4 shows the data and the fit. Ninety-one percent of the calculated:experimental ratios fall between 0.5 and 2.0, which is a slight improvement over the 86% obtained earlier with both Eqs. (10) and (13). It is a remarkable coincidence that the E^{-4} dependence derived by Bohr and Mottelson [Eqs. (11) and (12)] is also mandated by the data [Eq. (16)]. The exact A dependence is not critical; the best A dependence [Eq. (16)] is intermediate between A^1 of Grodzins [Eq. (10)] and $A^{1/3}$ of Bohr and Mottelson [Eq. (13)].

IV. LOCAL SYSTEMATICS

A. Systematics of Ross and Bhaduri

While Eqs. (10) and (13) predict the global trends, they are not very accurate, as can be seen from Figs. 3(a) and 3(b), respectively. However, these figures also show that the calculated:experimental lifetime ratios for neighboring nuclei do not differ much except near closed shells. This observation raises the possibility that more accurate local systematics may be developed from the experimental data. This was first done by Ross and Bhaduri.[6] After defining

$$F(N,Z) = [E \times B(E2)\uparrow]^{-1} , \quad (17)$$

these authors suggested that the value of $F(N,Z)$ for the anchor N,Z nucleus is related to the values for three neighboring nuclei by the difference equation

$$F(N,Z) + F(N+2,Z+2) - F(N+2,Z) - F(N,Z+2) \sim 0 . \quad (18)$$

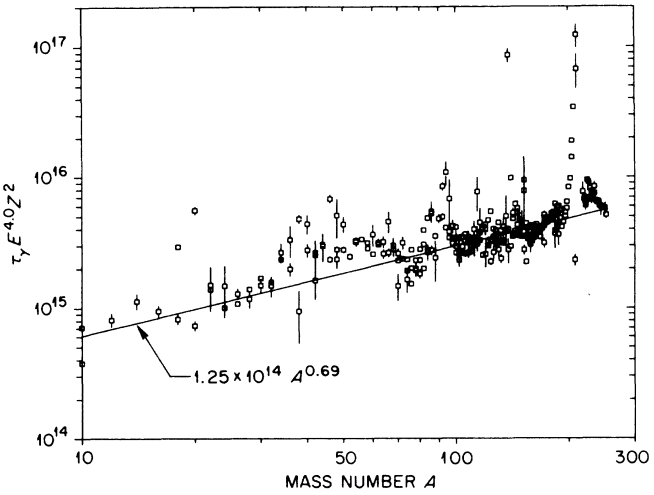

FIG. 4. Plot showing best overall fit [see Eq. (16)] to the γ-ray mean lifetime data excluding data for closed-shell nuclei.

If Eq. (18) is valid, it is possible to derive the F value for the fourth nucleus provided the F values for the three neighboring nuclei are known. Because the energies of the 2^+ states are invariably known long before their $B(E2)$ values, a knowledge of F leads to a $B(E2)$ prediction. The predicted $B(E2)$ values can be employed, in a bootstrap procedure, to yield still more $B(E2)$ values.

The origins of Eq. (18) trace back to the work of Bohr and Mottelson.[4] From their formulas [see Eqs. (4) and (5)] it follows that

$$F(N,Z)=C(\pi^2/\hbar^2 e^2 r_0^4)B_2 Z^{-2} A^{-4/3} , \tag{19}$$

where the constant C is $\frac{32}{45}$ for vibrational nuclei and $\frac{16}{9}$ for rotational nuclei. In the hydrodynamic model, the inertial mass parameter B_2 is given in terms of the nucleon mass M as

$$B_2=(3/8\pi)Mr_0^2 A^{5/3} . \tag{20}$$

Substitution of Eq. (20) into Eq. (19) leads to Eqs. (11) and (12) given earlier. Ross and Bhaduri replaced this estimate for B_2 with a more refined one based on the cranking model of Inglis.[14] The latter estimate incorporates the effects of single-particle motion plus pairing and hence is likely to reproduce the fluctuations about the smooth behavior predicted by the hydrodynamic model. Ross and Bhaduri showed that under reasonable assumptions, the cranking model formula for $B_2(N,Z)$ can be written in a separable form as

$$B_2(N,Z)\approx b_1(N)+b_2(Z) . \tag{21}$$

Using this expression, they found

$$F(N,Z)\propto [b_1(N)+b_2(Z)]Z^{-2}A^{-4/3} \tag{22}$$

for both spherical and deformed nuclei. The quantities $b_1(N)$ and $b_2(Z)$ may change appreciably with N and Z, but $Z^{-2}A^{-4/3}$ is smoothly varying and is approximately constant for the four nuclei appearing in the difference equation. Hence we may write

$$F(N,Z)\approx f_1(N)+f_2(Z) . \tag{23}$$

The difference equation, Eq. (18), immediately follows from Eq. (23).

We have tested this difference equation with the data in the $B(E2)$ compilation and obtained the results shown in Fig. 5(a). Except near closed shells, the deviations from zero are typically $\pm 30\%$ of the average of the four $B(E2)$ values. There are altogether 132 anchor nuclei, and 73% of these fall within this $\pm 30\%$ band.

B. Systematics of Patnaik, Patra, and Satpathy

It was noted by Patnaik, Patra, and Satpathy[7] that a difference equation similar to that proposed by Ross and Bhaduri[6] is also satisfied by E, the energy of the first 2^+ state, and by the reduced transition probability $B(E2)$. Thus they propose

$$E(N,Z)+E(N+2,Z+2)-E(N+2,Z)-E(N,Z+2) \sim 0 , \tag{24}$$

and

$$B(E2)[N,Z]+B(E2)[N+2,Z+2] -B(E2)[N+2,Z]-B(E2)[N,Z+2]\sim 0 . \tag{25}$$

Patnaik, Patra, and Satpathy[7] argued that the low-lying yrast states of a nonspherical nucleus can be described to a good approximation by states of definite angular momenta projected from an intrinsic state obtained self-consistently by a Hartree-Fock calculation. The difference equations follow if one assumes that the intrinsic state of N neutrons and Z protons is not altered very much by the addition of two neutrons or two protons.

As shown in Figs. 5(b) and 5(c), the difference equations (24) and (25) are well satisfied by the experimental data except near closed shells, where the $B(E2)$ values are comparatively low. The $B(E2)$ residuals fall within the $\pm 30\%$ band for 69% of the 132 cases. The difference equation for the energies for the first excited 2^+ states [Eq. (24)] works much better; 64% of the 316 cases (four-nuclei clusters) fall within the narrower $\pm 10\%$ band.

Another way to test these difference equations is to compare the predictions, made originally by the proponents of these equations, with new measurements. This is done in Table I. The overlap between the predicted and the measured values is good for 9 out of 16 entries. Doubling the uncertainty in either the predicted or the measured value extends this agreement to 13 out of 16 entries. Disagreements exist for ^{72}Se, ^{114}Pd, and ^{124}Xe, but the worst of these three, ^{114}Pd, is unusual because the predicted value for this nucleus is based on an extrapolated value for ^{112}Pd. If the measured value for ^{112}Pd (see column 4 of Table I) is employed, the predictions for ^{114}Pd in both columns 2 and 3 of Table I drop considerably to a value of 0.64 ± 0.10.

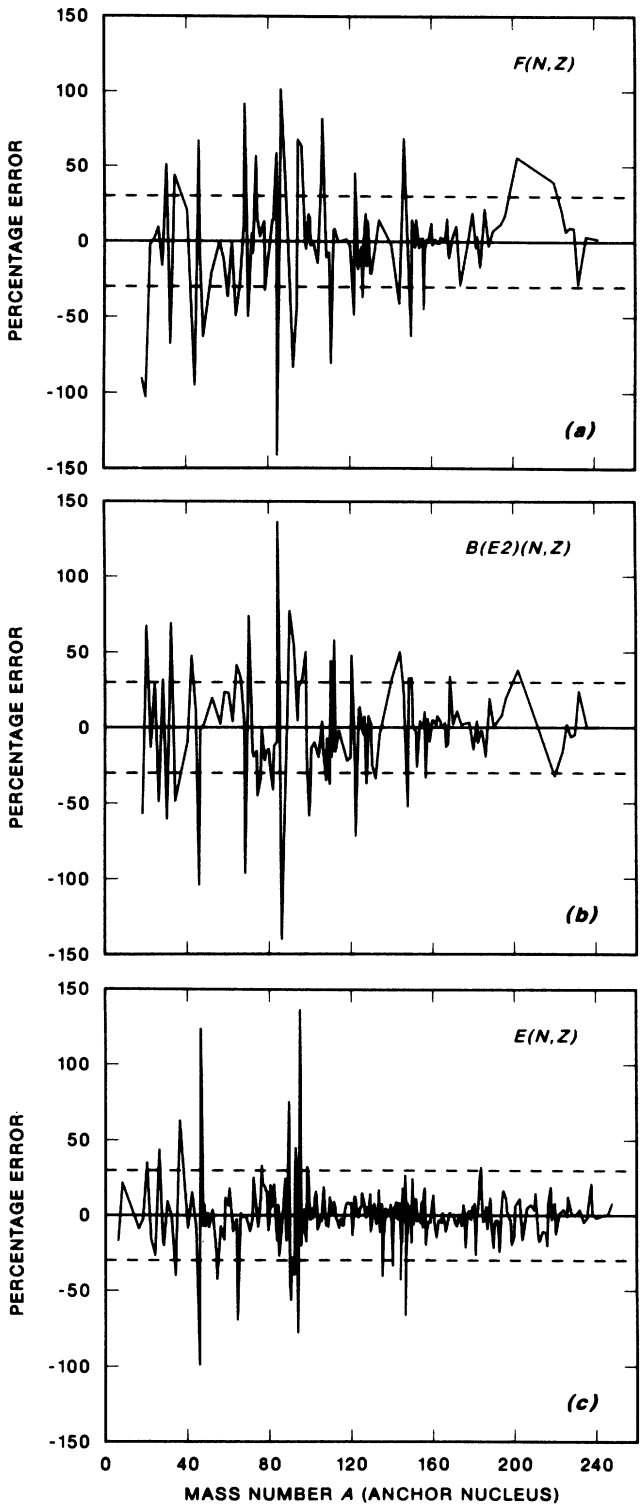

FIG. 5. Test of the difference equations of (a) Ross and Bhaduri [see Eq. (18) connecting F values for four adjacent nuclei], (b) Patnaik, Patra, and Satpathy [see Eq. (25) connecting $B(E2)\uparrow$ values], and (c) Patnaik, Patra, and Satpathy [see Eq. (24) connecting the energies of the first-excited 2^+ states]. The deviation from zero of the respective equation is divided by the average of the four values, expressed as a percentage, and plotted along the ordinate.

V. REGIONAL SYSTEMATICS

A. Systematics of Hamamoto

The notion that it is the neutron-proton (n-p) interaction that deforms nuclei is a key to understanding the midshell bumps in the $B(E2)$ values plotted in Fig. 1(b). Because the p-p and n-n interactions are predominantly of the pairing type, they cannot be responsible for the deformation of a nucleus. Pursuing this line of reasoning, Hamamoto[8] suggested more than two decades ago that the deformation is roughly proportional to the product N_pN_n, where the valence number of protons (neutrons) $N_p(N_n)$ is defined as the number of particles below midshell and the number of holes past midshell. It then follows that the $B(E2)$ values (for some fixed N_n values) would peak roughly midway between closed shells. In the $50 \leq Z \leq 82$ region, the $B(E2)$ values for the Gd, Dy, and Er isotopes with $N_p = 14$, 16, and 14, respectively, indeed show this type of behavior.

Hamamoto plotted the quantity $[\beta_2/\beta_{2(\text{s.p.})}]/N_pN_n$ as a function of Z and noted that this quantity was roughly constant over the entire mass region (both spherical and deformed) except for the regions near closed shells. The data available to her in 1965 were quite limited; she plotted 28 points in the $54 \leq Z \leq 78$ region. Our equivalent plot is shown in Fig. 6. There are now 90 data points in the same region and the ordinate values are no longer especially constant as a function of Z. Nevertheless, striking regularities are present in the data and to bring these out, we have plotted the quantity $[\beta_2/\beta_{2(\text{s.p})}]$ as a function of N_pN_n for nuclei in five different regions as shown in Fig. 7. The solid line in each figure is a fit to the data of the form [similar to Eq. (3) of Ref. 15]

$$\beta_2/\beta_{2(\text{s.p.})} = B + A(1 - e^{-\alpha N_n N_p}) , \tag{26}$$

where A, B, and α are constants. The smooth behavior is especially striking for isotopes heavier than Pb. The data point marked ^{152}Dy in Fig. 7(d) appears to be very low; this point is based on a single, unpublished measurement (see Table II of Ref. 1).

Figures 7(a) and 7(b) represent our attempts to extend these N_pN_n systematics to lighter regions where the data points are *a priori* expected to show wider scatter. In Fig. 7(b), the four data points for ^{90}Zr, ^{92}Zr, ^{94}Zr, and ^{96}Zr are low due to the subshell closure at $Z = 40$ and have been excluded in the fit. In an overall sense, the regional systematics shown in Fig. 7 appear to be capable of yielding a $\beta_2/\beta_{2(\text{s.p.})}$ prediction with an accuracy of about 10%, which translates to a $B(E2)$ prediction of about 20% accuracy.

B. Systematics of Casten

The investigations by Casten[9] of the correlations of $B(E2)$ values with the product N_pN_n of the valence protons and neutrons outside a closed shell is motivated by the same physical arguments used earlier by Hamamoto. Casten has broadened the N_pN_n systematics to include the energies of the first 2^+ states and the $E(4_1^+)/E(2_1^+)$ ratios; in fact the 2_1^+ and 4_1^+ energy systematics were his

TABLE I. Comparison of predicted and recently measured $B(E2)\uparrow$ values.

Nucleus	Ref. 6 Predictions $B(E2)\uparrow(e^2b^2)$	Ref. 7 Predictions $B(E2)\uparrow(e^2b^2)$	Ref. 1 Experiment $B(E2)\uparrow(e^2b^2)$
^{68}Ge		0.20±0.02	0.14±0.02
^{72}Se		0.44±0.08	0.18±0.03
^{102}Mo	1.05±0.15		1.06±0.12
^{104}Mo	1.56±0.32		1.08±0.08
^{106}Mo	1.74±0.50		1.30±0.07
^{108}Ru	1.25±0.20	1.08±0.15	1.03±0.14
^{110}Ru	1.23±0.25	1.12±0.18	1.11±0.13
^{112}Ru	1.28±0.35	1.19±0.22	1.12±0.20
^{112}Pd	0.90±0.10	0.90±0.09	0.63±0.10
^{114}Pd	0.97±0.13	0.96±0.10	0.34±0.10
^{124}Xe	0.99±0.14	1.10±0.07	1.49±0.09
^{146}Ce	1.07±0.10	1.05±0.07	0.93±0.13
^{148}Ce	1.82±0.20		1.89±0.15
^{152}Nd		3.64±0.18	2.6±0.7
^{182}Os	3.46±0.54	3.75±0.47	3.81±0.33
^{184}Os	3.41±0.35	3.54±0.23	3.20±0.15

starting points. When he arrived at the $B(E2)$ systematics, he discerned greater details and regularities in them. For example, Fig. 8(a) shows the data in the very broad Xe ($Z=54$) to Pb ($Z=82$) region with a straightforward method of counting N_p and N_n values based on the magic numbers. A subset of these data with a different method of deducing the N_p and N_n values is shown in Fig. 8(b). Casten[9] showed that the $B(E2)$ values split into two groups ($Z \leq 64$ and $Z \geq 66$). The $E(2_1^+)$ and the $E(4_1^+)/E(2_1^+)$ data behave in a similar manner. He provided a natural explanation for this behavior in terms of a significant subshell closure at $Z=64$. He also generated $B(E2)$ systematics in the $A \sim 100$ region[15] in which the protons fill either the 28–50 or the 38–50 shell and the neutrons fill the 50–82 shell. Tabor[16] extended these systematics to the $A \sim 80$ region in which neutrons and protons fill the same 28–50 shell.

Because we are interested here only in the overall systematics, we have reverted to the simple method of counting N_p and N_n values relative to the major magic numbers ($Z,N=28$, 50, 82, 126, and 184) and have plotted in Fig. 9 the $B(E2)$ systematics in five different regions. For reasons that will become clear in Sec. VI, we have omitted the data points for $N_p,N_n<4$. These data points (corresponding to $N_pN_n \leq 16$) have been included in the $\beta_2/\beta_{2(\text{s.p.})}$ plots shown in Fig. 7.

VI. UNDERSTANDING N_pN_n TRENDS

We now present three schematic models that attempt to explain the β_2 and $B(E2)$ trends shown in Figs. 7 and 9, respectively. The first is macroscopic and based on the SU(3) limit of the IBA. The second is microscopic and based on an SU(3) simulation of a major shell and the resulting symmetry properties. The last is also microscopic but based on a single large-j simulation of a major shell.

We consider nuclei that are not too close to shell boundaries. Thus we restrict ourselves to nuclei with four or more valence protons and neutrons and regard them as being "well deformed" in the sense that the low-lying states of the yrast band of such a deformed nucleus can be projected from a single intrinsic state.[17] In that case, the $B(E2)$ value is approximately proportional to the square of the intrinsic electric quadrupole moment Q_0,

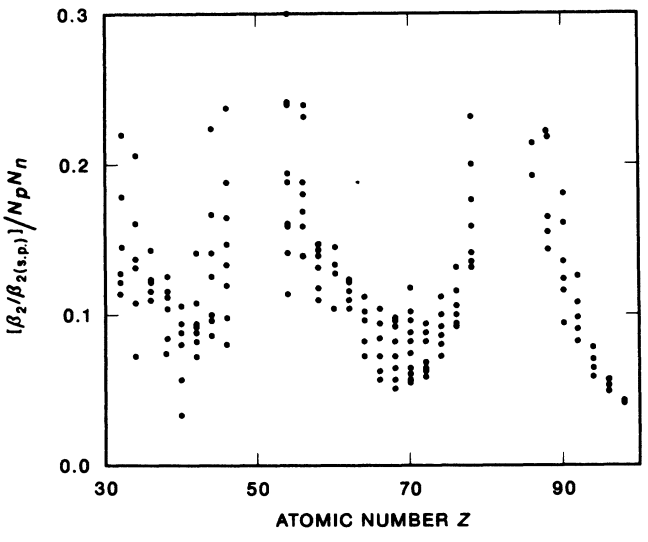

FIG. 6. The quadrupole deformation parameter β_2 is divided first by $\beta_{2(\text{s.p.})}$ ($=1.59/Z$) and the resulting quantity is divided by the product N_pN_n and plotted as a function of Z. Data points for $Z=48$, 50, 52, 80, 82, and 84 have been omitted. This plot is similar to Fig. 2 of Hamamoto (Ref. 8). The valence number of protons (neutrons) $N_p(N_n)$ is defined as the number of particles below midshell and the number of holes past midshell. The shells are based on the major magic numbers 28, 50, 82, 126, and 184.

$$B(E2)\uparrow \approx (5/16\pi)Q_0^2 \ . \tag{27}$$

We can write Q_0 as

$$Q_0 = e_p Q_p + e_n Q_n \ , \tag{28}$$

where Q_p and Q_n are the mass quadrupole moments of the valence protons and neutrons, respectively, in the intrinsic state of the nucleus, and e_p and e_n are the proton and neutron effective charges, respectively. We have to

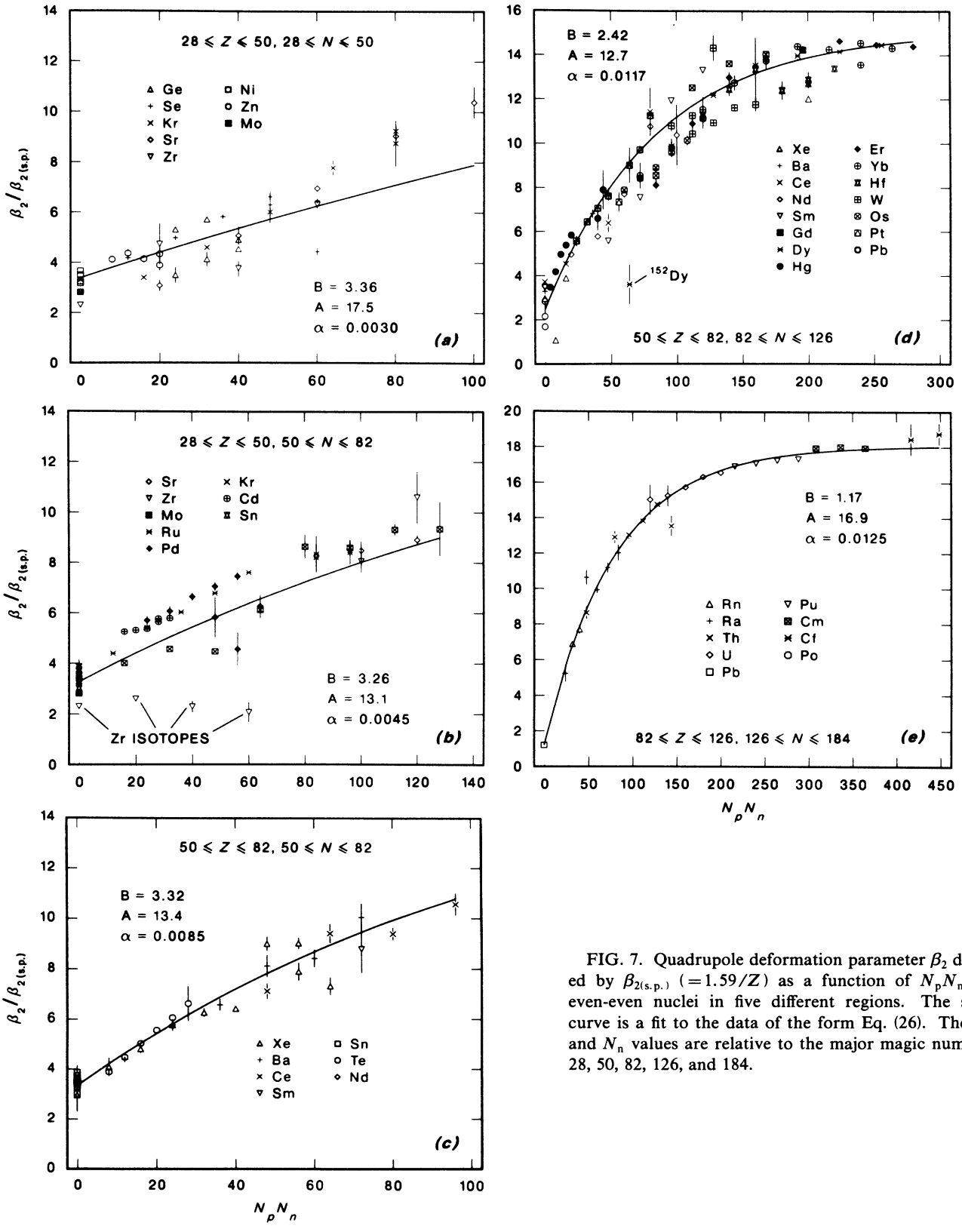

FIG. 7. Quadrupole deformation parameter β_2 divided by $\beta_{2(\text{s.p.})}$ $(=1.59/Z)$ as a function of N_pN_n for even-even nuclei in five different regions. The solid curve is a fit to the data of the form Eq. (26). The N_p and N_n values are relative to the major magic numbers 28, 50, 82, 126, and 184.

use the effective charges to simulate the contribution of the core, which is not entirely inert but is polarized by the valence nucleons. We consider two different approaches for calculating Q_p and Q_n as valence protons and neutrons are added to a nucleus.

A. Macroscopic SU(3) (IBA)

The first approach, based on the SU(3) limit of IBA, provides a direct, though approximate, insight into the N_pN_n trends. We assume that the yrast band of a well-deformed nucleus, to a good approximation, belongs to an SU(3) representation $(\lambda,0)$ where λ is equal to the maximum angular momentum of the band. In the IBA based on (s,d) bosons,

$$\lambda = J_{\max} = 2N_\pi + 2N_\nu = N_p + N_n \ , \tag{29}$$

where N_π (N_ν) is the number of valence proton bosons (neutron bosons). According to SU(3) algebra,[18] the states of different angular momenta corresponding to an SU(3) representation (λ,μ) can be projected from an intrinsic state and the mass quadrupole moment Q of the intrinsic state is proportional to $(2\lambda+\mu)$. Hence the mass quadrupole moment of an IBA SU(3) representation $(\lambda,0)$ can be written as

$$Q = CA^{1/3}(2\lambda) = CA^{1/3}2(N_p+N_n) = Q_p + Q_n \ , \tag{30}$$

where C (in units of b) is a constant. The $A^{1/3}$ factor is introduced to take into account the effect of the general increase in the size of the nucleus with the mass number. The intrinsic electric quadrupole moment is given by [see Eq. (28)]

$$Q_0 = CA^{1/3}2(e_pN_p + e_nN_n) \ . \tag{31}$$

This intrinsic state does not satisfy the Pauli principle exactly. If λ is not too small, the $B(E2)\uparrow$ value is given by [see Eq. (27)]

$$B(E2)\uparrow \approx (5/16\pi)C^2A^{2/3}4[e_pN_p + e_nN_n]^2 \ . \tag{32}$$

We write

$$B(E2)\uparrow \approx (4.07\times 10^{-5})A^{2/3}N_1^2[N_p + (e_n/e_p)N_n]^2 \ , \tag{33}$$

where N_1 (in units of eb) and (e_n/e_p) are constants to be determined by fitting this expression (see Sec. VI C) to the data in a particular region. The application of Eq. (33) to five different regions is shown in Fig. 9 by means of solid lines. The agreement between the calculated and measured trends is quite adequate except in the actinide region. The main point to emerge from these comparisons is that the physical parameter governing the $B(E2)\uparrow$ behavior is $(e_pN_p+e_nN_n)^2$ and not N_pN_n. In the actinide region, the IBA schematic model predicts $B(E2)\uparrow$ values that increase with N_pN_n, whereas the experimental $B(E2)\uparrow$ values show saturation [see Fig. 9(e)].

From Fig. 9 it appears that Eq. (33) is adequate for explaining several regional $B(E2)$ trends. For deformed nuclei that can be described by the SU(3)-O(6) limits of IBA, the $B(E2)$ values are given exactly[19] by the expressions

$$\mathrm{O(6)}: B(E2)\uparrow = \left[\frac{N+4}{N}\right](e_\nu N_\nu + e_\pi N_\pi)^2 \tag{34}$$

and

$$\mathrm{SU(3)}: B(E2)\uparrow = \left[\frac{2N+3}{N}\right](e_\nu N_\nu + e_\pi N_\pi)^2 \ , \tag{35}$$

where e_π (e_ν) is the proton (neutron) boson effective

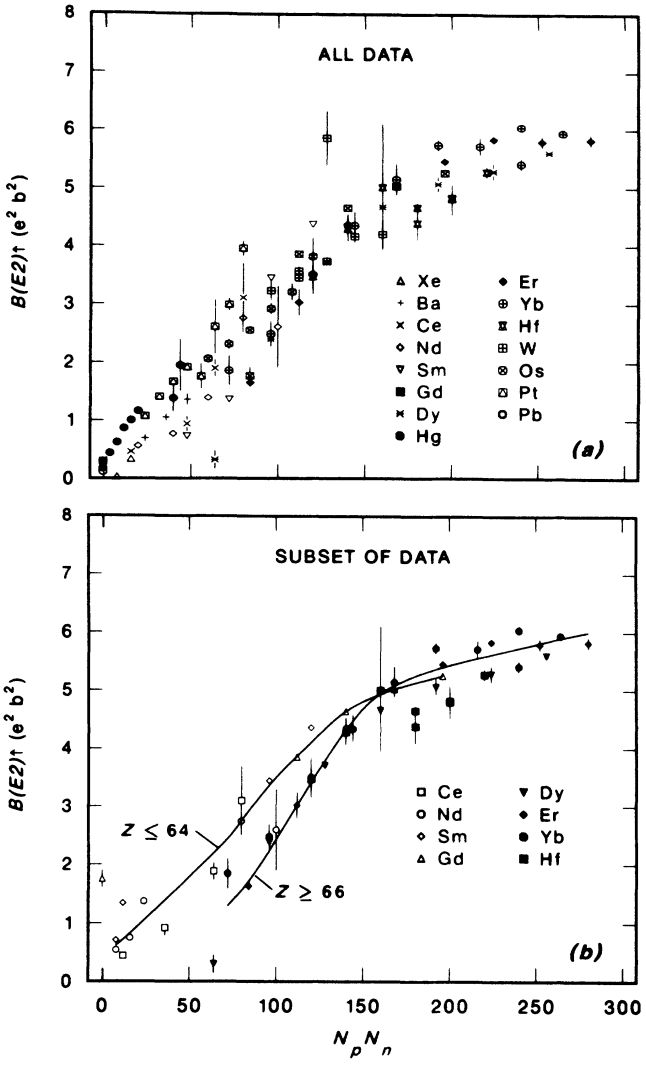

FIG. 8. Systematics of $B(E2)$ values in the $A \approx 150$ region. The bottom plot is similar to Fig. 24 of Casten (Ref. 9). The curves are fits to the data of the form Eq. (26). To construct the abscissa values, Casten (Ref. 9) employed the following definitions: (a) for $Z \leq 64$ and $N < 90$, the proton shell is 50–64; (b) for $Z \leq 64$ and $N \geq 90$, the proton shell is 50–82; (c) for $Z \geq 66$, the neutron shell is 82–126 and the proton shell is 50–82. We have adopted these definitions in constructing the bottom part of this figure. The top part is based on the standard $Z = 50$–82 and $N = 82$–126 definition of the shells.

charge in units of eb and N_π (N_ν) is the number of proton (neutron) bosons. The sum of N_π and N_ν is denoted by N. We expect the ratio of the boson effective charges (e_ν/e_π) to be equal to the ratio of the nucleon effective charges (e_n/e_p). On the basis of the above expressions, Casten and Wolf[20] have suggested a single empirical formula that interpolates between the SU(3) and O(6) limits. Their formula is

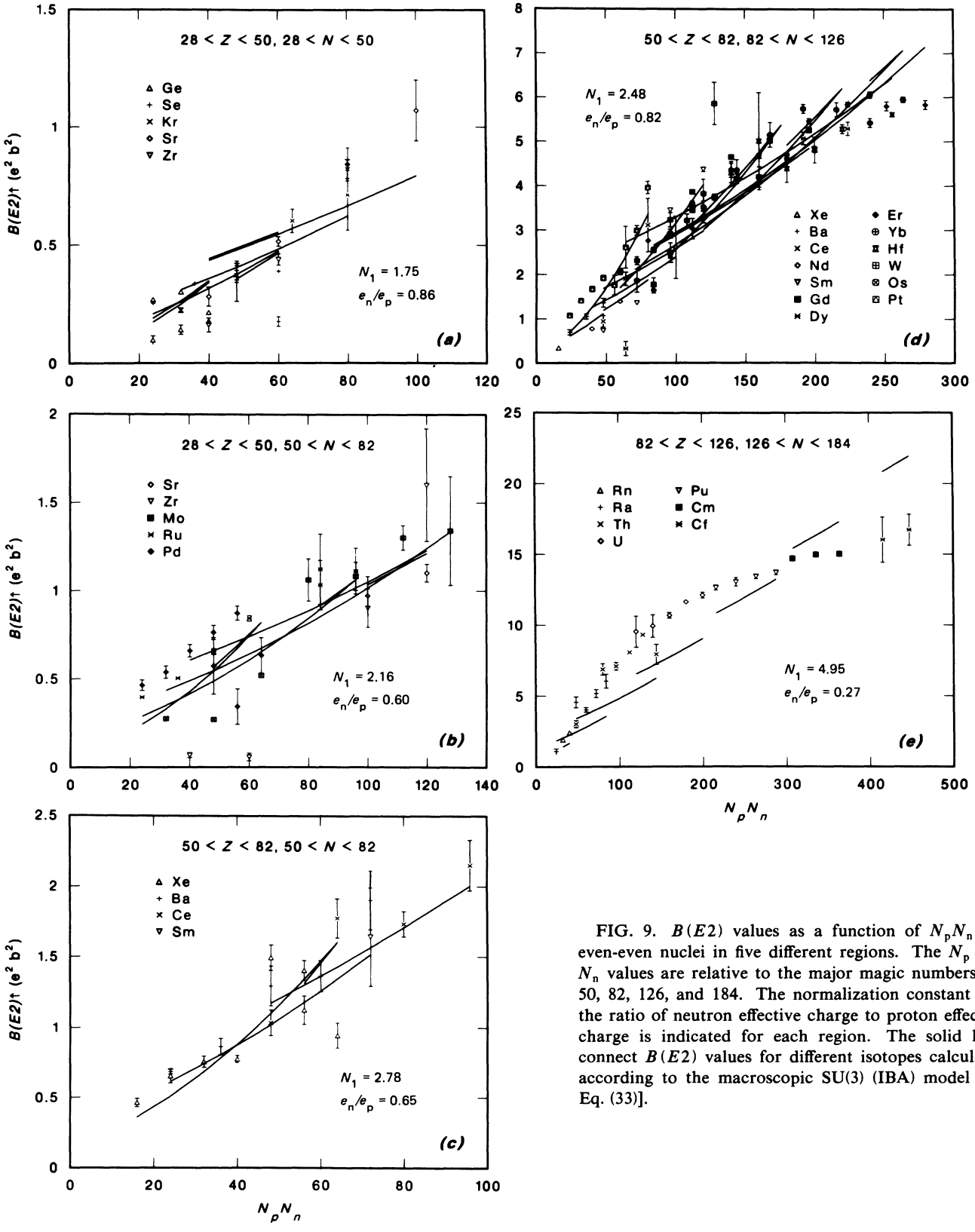

FIG. 9. $B(E2)$ values as a function of N_pN_n for even-even nuclei in five different regions. The N_p and N_n values are relative to the major magic numbers 28, 50, 82, 126, and 184. The normalization constant and the ratio of neutron effective charge to proton effective charge is indicated for each region. The solid lines connect $B(E2)$ values for different isotopes calculated according to the macroscopic SU(3) (IBA) model [see Eq. (33)].

$$B(E2)\downarrow = C^2 \left[\frac{N+1}{N} \right]^2 (e_\nu N_\nu + e_\pi N_\pi)^2 , \quad (36)$$

where $C = 0.5(1 - 0.1\chi)$ is given in terms of the IBA quadrupole operator parameter χ determined by fitting the level energies. This parameter varies over the range $-1 < \chi < 0$. Casten and Wolf[20] claim that Eq. (36) gives values that are within $\pm 12\%$ of detailed numerical IBA calculations that had been shown earlier[15] to reproduce the general trends of $B(E2)$ values in the $A = 100-200$ region.

B. Microscopic models

We now consider a microscopic approach to understanding the observed $B(E2)$ trends. Bohr and Mottelson[21] and Otsuka, Arima, and Iachello[22] have attempted to analyze the nature of collective states in nuclei by replacing a shell consisting of many j single-particle states with a shell of just one large j value. In a similar spirit, we simulate the different shells in two ways: (1) single-particle SU(3) representation, and (2) large single-j representation. In both cases, the degeneracy is chosen to be approximately the same as that of the shell under consideration.

Consider, for example, the $N,Z = 50-82$ shell. The total number of single-particle states required in this shell is 32. We simulate this shell by a schematic "*s-d-g*" shell corresponding to the (4,0) representation of SU(3). This SU(3) shell contains $2(1+5+9) = 30$ single-particle states rather than the required 32; we ignore this small difference. We also simulate the 50–82 shell with a single $j = \frac{31}{2}$ shell with 32 states. Similarly, we replace the 82–126 shell with a "*p-f-h*" SU(3) or a $j = \frac{43}{2}$ shell, and the 126–184 shell with a "*s-d-g-i*" SU(3) or a $j = \frac{57}{2}$ shell. Although these simulations are expected to be reasonable only for shells with large degeneracies, we also consider the $N,Z = 28-50$ shell and simulate this shell with a "*p-f*" SU(3) representation that has the right approximate degeneracy. This "*p-f*" representation is actually more appropriate for the $N,Z = 20-40$ shell.

1. Single-particle "SU(3)"

We are interested in estimating the intrinsic mass quadrupole moments Q_p and Q_n of the valence protons and neutrons in order to evaluate the intrinsic electric quadrupole moment Q_0 [see Eq. (28)]. On the basis of Hartree-Fock calculations[23–27] in the *s-d*, *f-p*, and *f-p-g* ($g_{9/2}$ only) shells, and from the relative constancy of the slopes (beyond, say, $\beta_2 \approx 0.15$) of the majority of the Nilsson levels[28] throughout the periodic table, we conclude that the mass quadrupole moments are close to their asymptotic values within their respective shells. These values are just the eigenvalues

$$q_k = \langle k \mid Q_0^{(2)} \mid k \rangle \quad (37)$$

of the single-particle mass quadrupole moment operator. The q_k values for the deformed eigenstates $\mid k \rangle$ of $Q_0^{(2)}$ for the "*s-d-g*" shell are proportional to 8, 5, 2, -1, and -4. The constant of proportionality is the oscillator parameter α^2 ($= \hbar/M\omega$) for an oscillator SU(3) model. We retain α^2 as the appropriate unit and include an adjustable parameter in our model. The spectrum of $k = \langle l_z \rangle$ and the associated q_k values are sketched in Fig. 10 for the "*s-d-g*" shell simulation of the $N,Z = 50-82$ region and for similar simulations of the three other shells.

Figure 11 shows the method of constructing the intrinsic state and estimating the Q_p and Q_n values for a typical nucleus $^{118}_{56}Ba_{62}$. The six valence protons occupy the three orbits with $k = 0$ and ± 1 with q_k values of 8 and 5 units, respectively. The twelve valence neutrons occupy the orbits with $k = 0$, $(-1, +1)$, and $(-2, 0, +2)$ with q_k values of 8, 5, and 2 units, respectively. In this manner, the Pauli principle is explictly taken into account. The resulting Q_p and Q_n values are given in Fig. 11. The intrinsic electric quadrupole moment is now

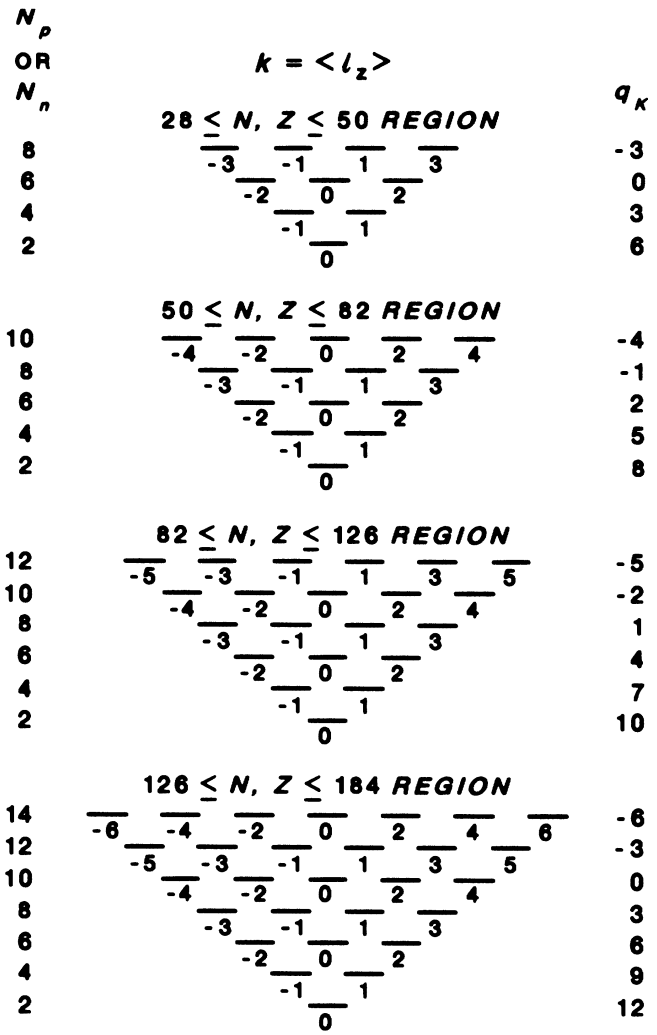

FIG. 10. Schematic single-particle SU(3) simulation of the major shells. The number of protons (neutrons) is denoted by $N_p(N_n)$, the deformed eigenstate by k, and the eigenvalues of the single-particle mass quadrupole moment operator by q_k. The q_k values are in units of α^2, where $\alpha^2 = \hbar/M\omega$ is the oscillator parameter.

given by [see Eq. (28)]

$$Q_0 \propto (e_p 36 + e_n 48)\alpha^2 , \quad (38)$$

where α^2 has the numerical value of $0.0101 A^{1/3}$b. We write the corresponding $B(E2)\uparrow$ value (in units of e^2b^2) as

$$B(E2)\uparrow \approx (1.02\times 10^{-5}) A^{2/3} N_2^2 [36 + (e_n/e_p)48]^2 . \quad (39)$$

We generalize by writing

$$B(E2)\uparrow \approx (1.02\times 10^{-5}) A^{2/3} N_2^2 [Q_p + (e_n/e_p)Q_n]^2 , \quad (40)$$

where N_2 and (e_n/e_p) are constants to be determined by fitting the calculated values to the experimental data in a particular region (see Sec. VI C). The resulting fits and the corresponding N_2 and (e_n/e_p) values are shown in Fig. 12. The agreement between the calculated and measured trends is again quite adequate in all except the lightest region [Fig. 12(a)]. In the case of the actinides, the predictions of the single-particle SU(3) model agree better with the data [see Fig. 12(e)] than those of the macroscopic SU(3) IBA model [see Fig. 9(e)]. In particular, the measured $B(E2)$ values for Cm ($Z=96$, $N=148$, 150, and 152) and Cf ($Z=98$, $N=152$ and 154) isotopes remain approximately constant. The calculated values reproduce this trend because neutrons in the 148–158 region are filling orbits with $q_k=0$ (see Fig. 10, $126 \le N$, $Z \le 184$ region) and therefore not causing a net increase in the Q_0 or $B(E2)$ values. There is also a hint of saturation in the deformed rare earth region [see Fig. 12(d)]. By contrast, the $B(E2)\uparrow$ values tend not to saturate in the macroscopic SU(3) IBA model [see Eq. (33) and Figs. 9(d) and 9(e)].[29]

The observed $B(E2)$ trends in the $N,Z=28$–50 region are not reproduced well [see Fig. 12(a)] by the single-particle SU(3) model. The reason for this failure is related to the rapid rise in the deformation[30–32] of nuclei with proton and neutron numbers in the 34–42 range. The effective shell size for these nuclei is known to be much larger than that assumed in the "SU(3)" model with only 20 single-particle states. The effective shell sizes assumed for the remaining regions, on the other hand, appear to be adequate to describe their deformation trends.

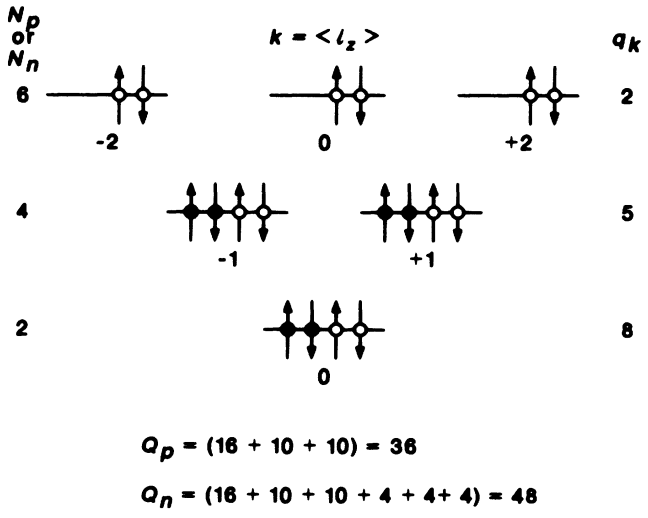

FIG. 11. Proton and neutron occupations of eigenstates for a typical nucleus $^{118}_{56}Ba_{62}$ and the estimation of the corresponding Q_p and Q_n values in units of the oscillator parameter α^2.

2. *Single-j simulation*

The lowest-energy, single-determinant intrinsic state of nucleons filling a single-j shell has an oblate shape. We do not choose this state because nuclei are generally prolate. Instead we consider the lowest-energy, axially symmetric, prolate intrinsic state in the j^n space. We can construct such a state by sequentially adding nucleons to orbits characterized by $k=\pm 1/2$, $\pm 3/2, \ldots, \pm j$. The expectation values of the mass quadrupole moments for the different $|k\rangle$ orbits,

$$q_k = \langle jk \,|\, Q_0^{(2)} \,|\, jk \rangle , \quad (41)$$

are proportional to the Clebsch-Gordan coefficients $\langle j2k0 \,|\, jk \rangle$. The Q_n or Q_p values, obtained by adding up the q_k values for the occupied orbits, are given in Table II for nucleons in the $j=\frac{31}{2}$, $\frac{43}{2}$, and $\frac{57}{2}$ shells. These values are in the same units as those for the SU(3) states also given in this table. They are normalized to the SU(3) values at N_p (or N_n) values of 12, 20, and 28 for the $j=\frac{31}{2}$, $\frac{43}{2}$, and $\frac{57}{2}$ shells, respectively.

With the aid of Table II we calculate the $B(E2)$ values in the same manner as before. We write [cf. Eq. (40)]

$$B(E2)\uparrow \approx (1.02\times 10^{-5}) A^{2/3} N_3^2 [Q_p + (e_n/e_p)Q_n]^2 . \quad (42)$$

The results are shown in Fig. 13. The agreement with the data is comparable to the SU(3) simulation.

C. Effective charges

We discuss here how the effective charge ratios e_n/e_p given in Figs. 9, 12, and 13 were chosen. Mottelson[33,34] has shown that the effective charges resulting from the quadrupole polarization of the "core" are given by $e_p=[(A+Z)/A]e$ and $e_n=(Z/A)e$. The ratio $e_n/e_p=Z/(A+Z)$ changes slowly from nucleus to nucleus, always hovering around 0.3. In our fits to the $B(E2)$ values, we find that if we use the above prescription we generally obtain a much larger spread in the calculated $B(E2)$ values (for nuclei corresponding to a fixed value of N_pN_n) than is warranted by the data. We therefore prefer to treat e_n/e_p as a parameter, whose values in different regions are to be determined by fits to the experimental $B(E2)$ values, the calculated values being generated by Eqs. (33), (40), and (42) corresponding to the three different models. We ignore the expected small variations in this ratio and try to find a single value for e_n/e_p for each region.

To determine the optimum e_n/e_p value for each of the

five shells shown in Figs. 9 and 12 and for the three shells shown in Fig. 13, we proceed as follows. In a given shell, we calculate the $B(E2)$ values for a number of values for the ratio e_n/e_p ranging from 0 to 1. For each value of e_n/e_p, we determine the sum of the squares of the differences between the calculated and measured $B(E2)$ values for all nuclei in the shell. Figure 14 shows the variation of this sum as a function of

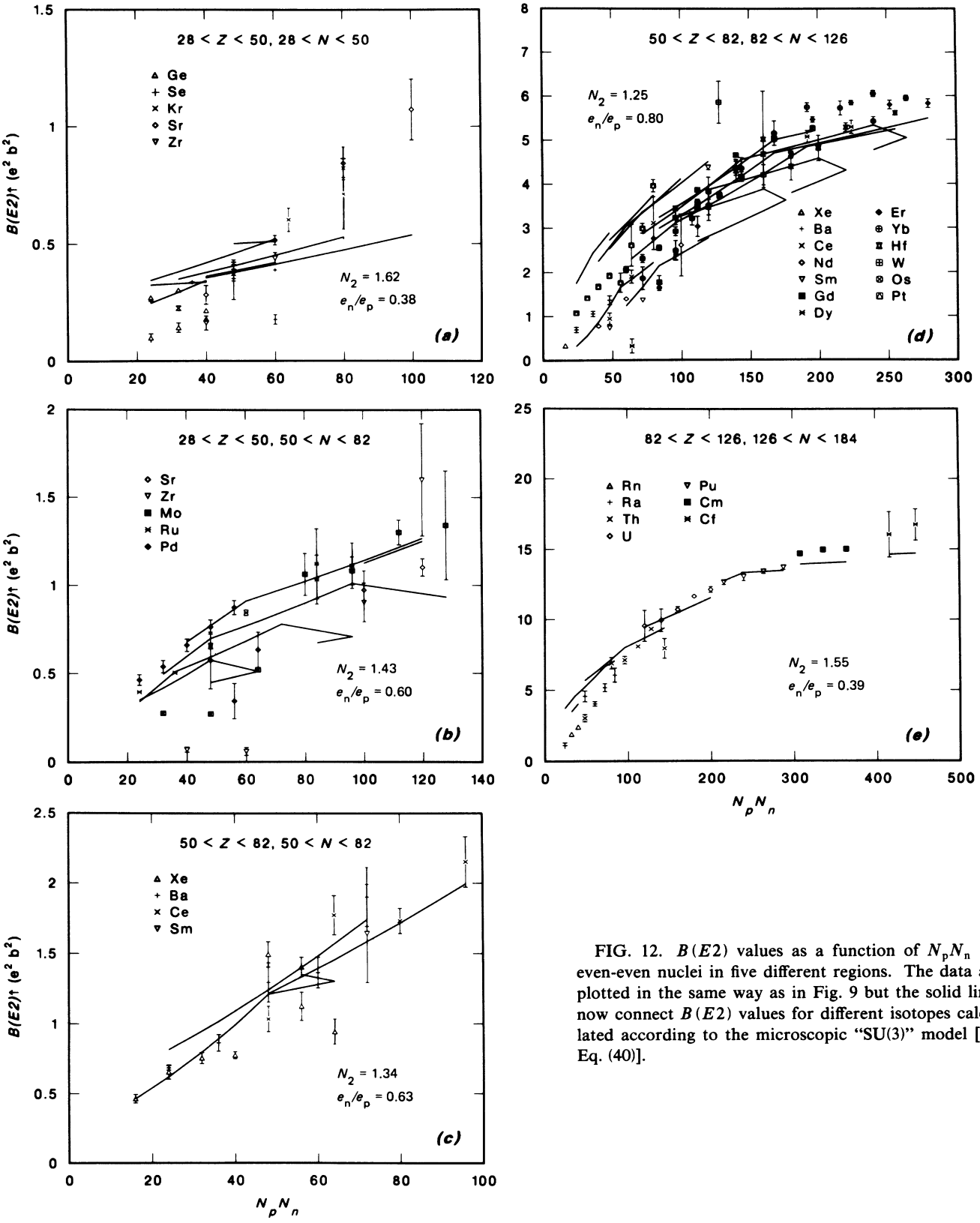

FIG. 12. $B(E2)$ values as a function of N_pN_n for even-even nuclei in five different regions. The data are plotted in the same way as in Fig. 9 but the solid lines now connect $B(E2)$ values for different isotopes calculated according to the microscopic "SU(3)" model [see Eq. (40)].

TABLE II. Mass quadrupole moments Q_p (Q_n) of protons (neutrons) for various shells. The quadrupole moments are in units of the oscillator parameter $\alpha^2=\hbar/M\omega=1.01\times10^{-2}A^{1/3}$b. The moments for the $j=\frac{31}{2}$, $\frac{43}{2}$, and $\frac{57}{2}$ shells are normalized (indicated by underlines) to be equal to those for the s-d-g, p-f-h, and s-d-g-i shells at $N_p(N_n)=12$, 20, and 28 respectively.

	50–82		82–126		126–184	
$N_p(N_n)$	$(\frac{31}{2})^N$	$(s\text{-}d\text{-}g)^N$	$(\frac{43}{2})^N$	$(p\text{-}f\text{-}h)^N$	$(\frac{57}{2})^N$	$(s\text{-}d\text{-}g\text{-}i)^N$
2	9.3	16	10.0	20	11.1	24
4	18.3	26	20.0	34	22.2	48
6	26.9	36	29.7	48	33.1	60
8	34.9	40	39.0	56	43.8	72
10	42.0	44	47.8	64	54.2	84
12	48.0	48	56.0	72	64.1	96
14	52.8	46	63.4	74	73.6	102
16	56.0	44	70.0	76	82.6	108
18	57.4	42	75.6	78	90.9	114
20	56.8	40	80.0	80	98.5	120
22	54.1	32	83.2	76	105.3	120
24	49.0	24	85.0	72	111.1	120
26	41.3	16	85.3	68	116.1	120
28	30.7	8	84.0	64	120.0	120
30	17.0	0	80.9	60	122.8	120
32	0		76.0	50	124.3	114
34			69.0	40	124.7	108
36			59.9	30	122.2	102
38			48.6	20	119.7	96
40			35.0	10	115.7	90
42			18.9	0	110.1	84
44			0		102.9	72
46					93.9	60
48					83.1	48
50					70.3	36
52					56.6	24
54					38.8	12
56					19.8	0
58					0	

e_n/e_p for the three models. Except in 3 out of 13 cases, the e_n/e_p ratios employed in Figs. 9, 12, and 13 are those that give a minimum, however shallow, in Fig. 14. The $Z=28-50$, $N=50-82$ curves decrease monotonically [see Figs. 14(a) and (b)], and we have elected to show the calculated curves corresponding to $e_n/e_p=0.60$ for these two cases in Figs. 9(b) and 12(b). The $Z=50-82$, $N=82-126$ curve behaves similarly [see Fig. 14(b)] and the calculated curves shown in Fig. 12(d) correspond to $e_n/e_p=0.80$.

Once the e_n/e_p value for a particular region is chosen, a separate least-squares fit yields the other parameter N_1 in Eq. (33). The same procedure applies for N_2 in Eq. (40) and N_3 in Eq. (42). The N_1, N_2, and N_3 values are also given explicitly in the different frames of Figs. 9, 12, and 13.

To clarify the effect of e_n/e_p on the goodness of fit, consider the $Z=50-82$, $N=82-126$ region. If we employ the IBA SU(3) model, we obtain via Eq. (33) the three sets of curves shown in Fig. 15 for e_n/e_p ratios of 0.30, 0.82, and 1.0. It is clear that a small value of e_n/e_p, close to the value prescribed by Mottelson, gives rise to a family of $B(E2)$ curves (upper panel of Fig. 15) that is considerably wider than the data. This family is narrower for $e_n/e_p=1.0$ (bottom panel of Fig. 15) but is most compact when $e_n/e_p=0.82$ (middle panel of Fig. 15). The middle choice is then shown in Fig. 9(d).

VII. GLOBAL CALCULATIONS

We consider here two detailed calculations of equilibrium deformations carried out throughout the periodic table within the framework of two different theoretical models. The first one by Kumar[12] uses a microscopic dynamic deformation model in which the nuclear shapes as well as spectroscopic properties of nuclei are calculated using a schematic pairing plus quadrupole effective interaction. Results are available[35–40] for only about 65 nuclei from $A=10$ to $A=250$. The calculated values are compared with the experimental ones (whenever possible) in Fig. 16(b).

Möller and Nix[10,11] have developed a macroscopic-microscopic model to calculate the masses and equilibrium shapes of nuclei throughout the periodic table (excluding nuclei lighter than ^{16}O). They have based their calculation on the macroscopic liquid-drop model to take into account the major part of the ground state

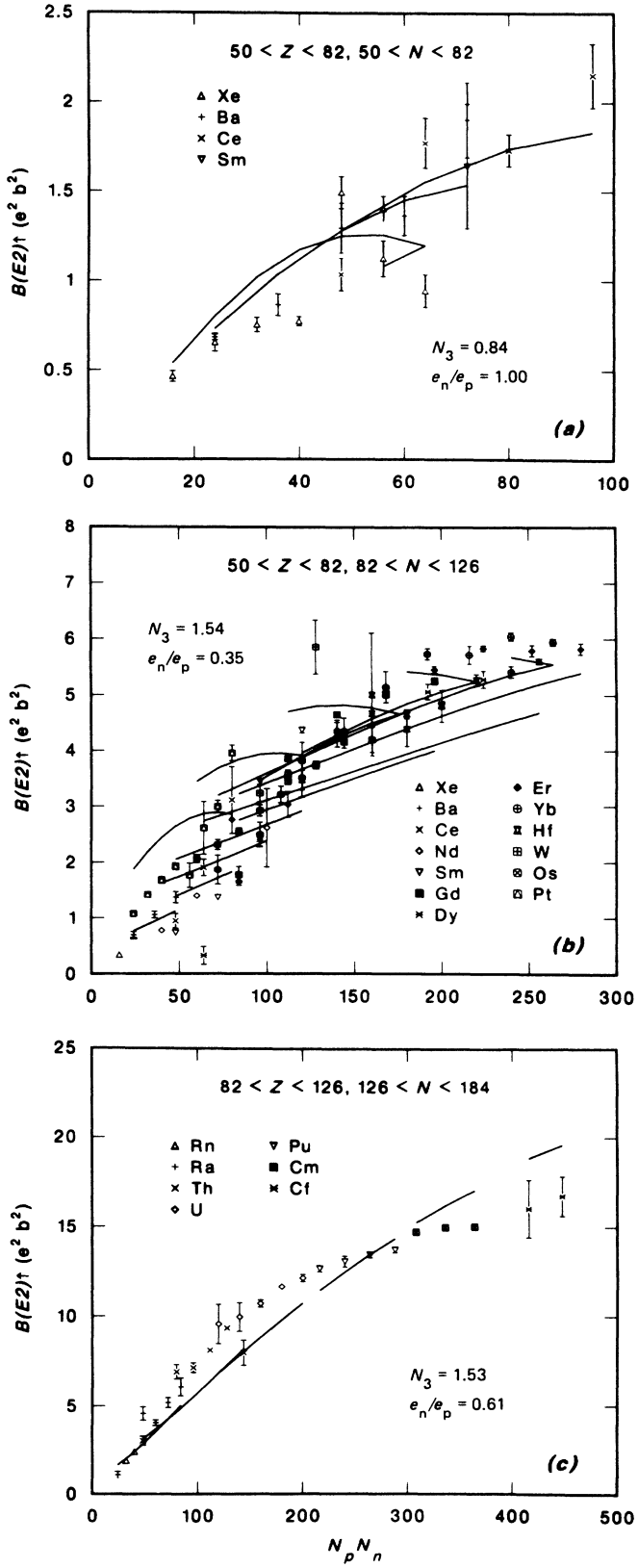

FIG. 13. $B(E2)$ values as a function of N_pN_n for even-even nuclei in three different regions. The data are plotted in the same way as in Figs. 9 and 12, but the solid lines now connect $B(E2)$ values for different isotopes calculated according to the microscopic large single-j model [see Eq. (42)].

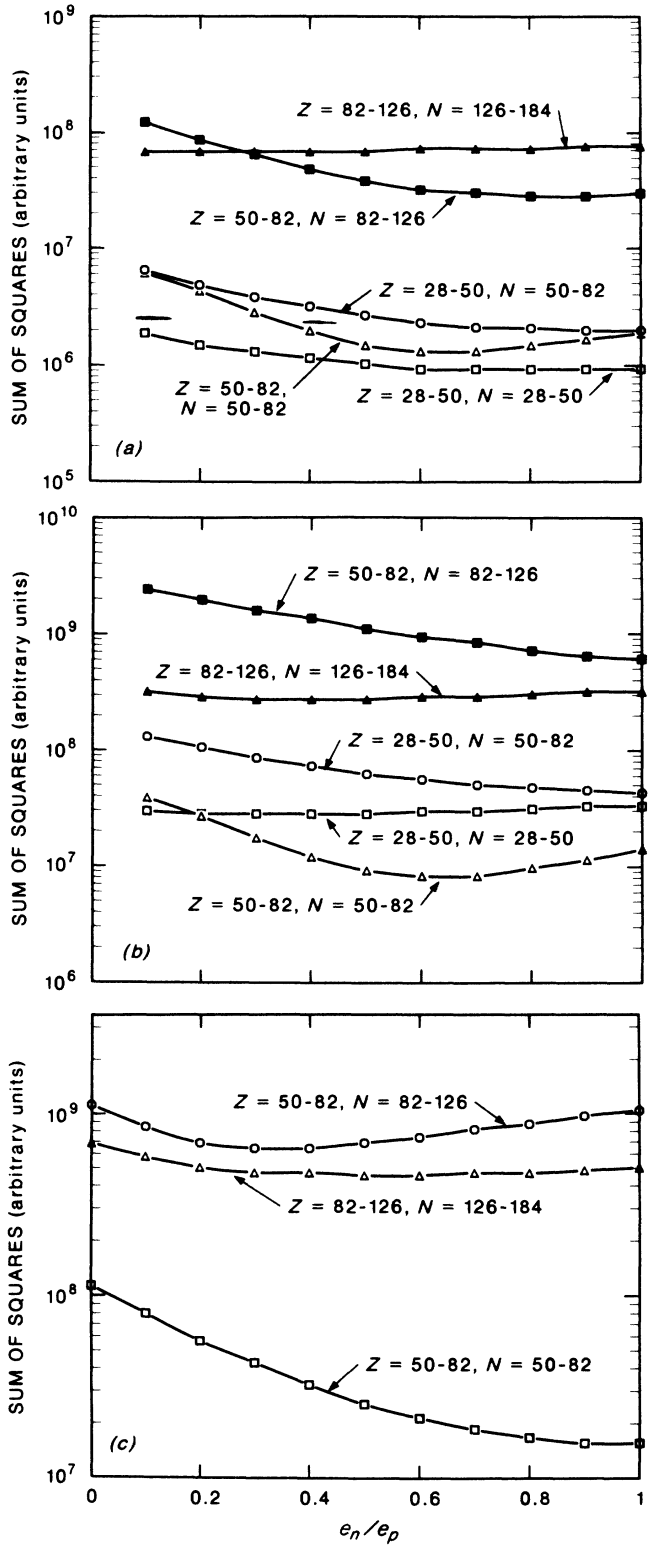

FIG. 14. Sum of the squares of the differences between the calculated and measured $B(E2)$ values vs ratio of the neutron and proton effective charges treated as a parameter. The calculations use (a) Eq. (33) of the macroscopic SU(3) model, (b) Eq. (40) of the microscopic "SU(3)" model, and (c) Eq. (42) of the microscopic large single-j model.

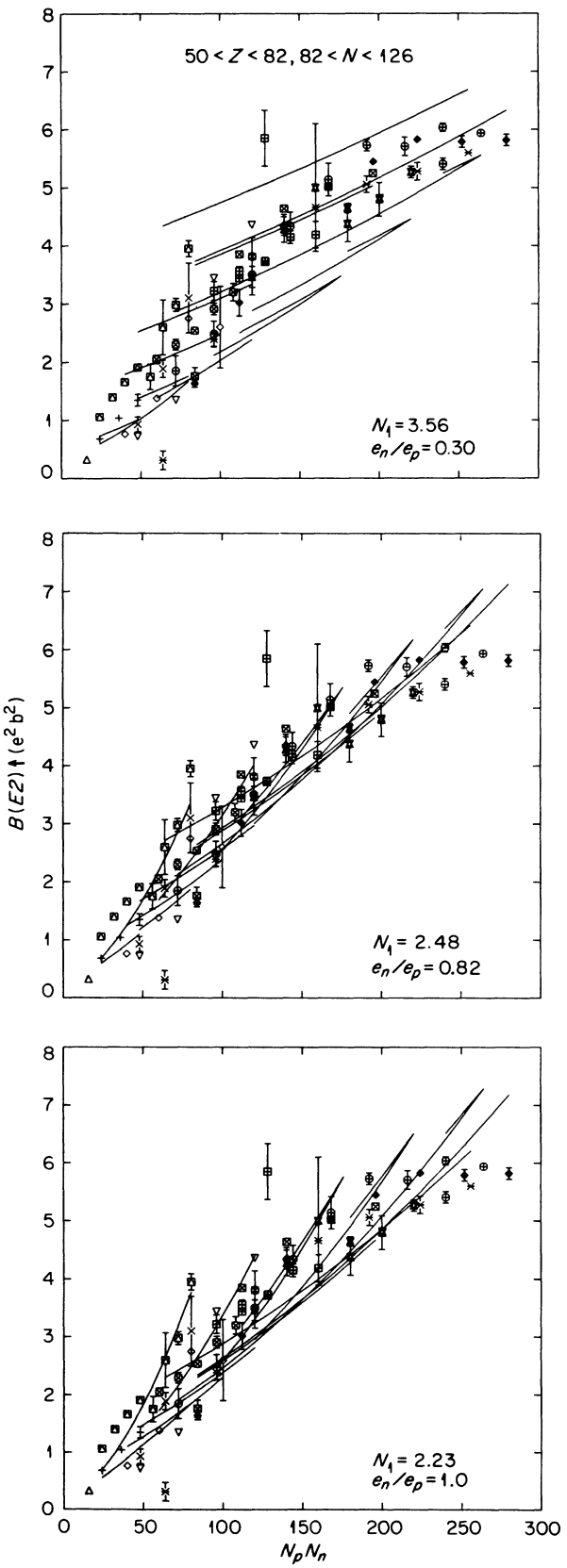

FIG. 15. Effect of changing e_n/e_p ratios on the calculated $B(E2)$ values (solid lines). The calculations use Eq. (33) of the macroscopic SU(3) model.

mass of the nucleus. This model is then appropriately and extensively extended to take into account the corrections due to the effects of the finite diffuseness of the surface, finite curvature of the surface, shell structure, and pairing. The nuclear shape is allowed to have Q_2 and Q_4 deformations. The equilibrium deformation of the nucleus is determined by minimizing the total macroscopic and microscopic potential energy of each nucleus as a function of the shape parameters ε_2 and ε_4. The absolute values of the intrinsic quadrupole moments of the equilibrium shapes of nuclei calculated by Möller and Nix[10] are compared (whenever possible) with the experimental values in Fig. 16(a). The underprediction in the theory might be related to the neglect of dynamic deformation effects.

Finally, we note that in addition to these two calculations, Vautherin[41] has carried out Hartree-Fock calculations for a few light and rare earth nuclei using the Skyrme interaction. These calculations reproduce the intrinsic electric quadrupole moments of these nuclei quite well.

VIII. DISCUSSION AND SUMMARY

The recent completion of a comprehensive compilation of $B(E2,0_1^+ \rightarrow 2_1^+)$ values for even-even nuclei has provided us with a unique opportunity to examine different ways of systematizing these values and related quantities. The γ-ray mean lifetimes vary over nine decades (10^{-3}–10^6 psec), yet show strikingly regular global behavior (Fig. 2) when plotted against three decades of energies (0.04–7 MeV) of the first 2^+ states. These lifetimes can be reproduced (to within a factor of 2) by relatively simple expressions anchored on sound physical principles.

The available data indicate, nay mandate, that the γ-ray mean lifetimes of the first 2^+ states vary with the energies E of these states as E^{-4} [see Eq. (16)]. This behavior for these collective states of nuclei is expected from the hydrodynamic model. In this model, the E^{-4} dependence essentially follows from the assumptions that for spherical nuclei the vibrations are harmonic and for deformed nuclei the moment of inertia of the intrinsic state is proportional to the square of the deformation. Because neither of these assumptions is strictly valid, we might have expected to observe some deviations from a strict E^{-4} dependence. It is, therefore, a bit surprising that we failed to do so.

The dependence of the lifetimes on the mass number A is far less stringent. The best fit to the data indicates an $A^{0.69}$ dependence, but an $A^{1/3}$ dependence suggested by the hydrodynamic model or an A^1 dependence suggested empirically on the basis of an earlier smaller $B(E2)$ compilation would work nearly as well. The $A^{1/3}$ dependence in the hydrodynamic model arises [see Eqs. (4) and (5)] from the combined effect of an $A^{1/3}$ dependence of the nuclear radius, which is empirically well established, and an $A^{5/3}$ dependence of the inertial mass parameter, which is less well established. Any deficiency in the latter could explain any slight breakdown of the $A^{1/3}$ dependence.

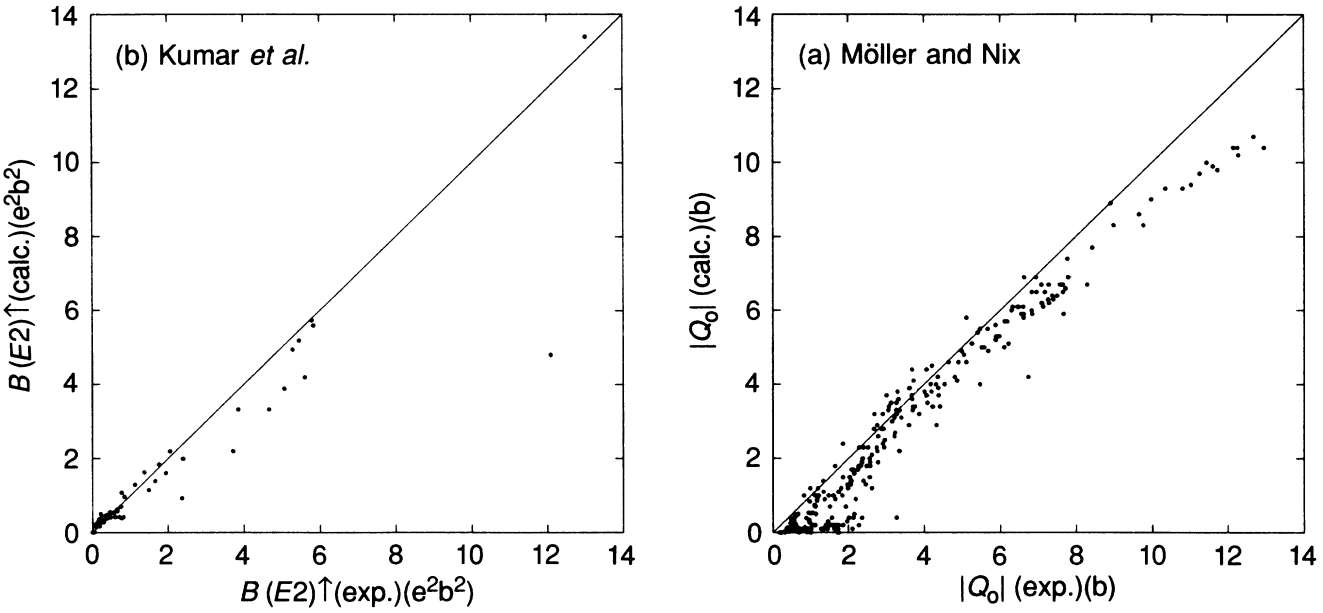

FIG. 16. (a) Experimentally determined (Ref. 1) intrinsic electric quadrupole moments $|Q_0|$ for 278 nuclei compared with the predictions of Möller and Nix (Ref. 10). (b) Experimentally determined (Ref. 1) $B(E2)\uparrow$ values for 55 nuclei compared with the calculations of Kumar and his co-workers (Refs. 12 and 35–40).

The local regularities in the $B(E2)$ values are such that simple closure relationships apply. These relationships can be employed to make reasonable predictions (good to about $\pm 30\%$) of unmeasured $B(E2)$ values. A number of such predictions, made more than a decade ago, have been borne out by recent measurements.

The compilation of $B(E2)$ values has helped to establish clearly the smooth dependence of nuclear deformation (see Fig. 7) on the product $N_p N_n$ of the valence protons and neutrons throughout different regions of the periodic table and especially for the heavier nuclei. An empirical formula has been developed [Eq. (26)] that predicts the deformation parameter β_2 of a nucleus with an accuracy of about $\pm 10\%$, which translates to a $B(E2)$ prediction of $\pm 20\%$ accuracy. This formula has three constants and a simple method of counting N_p and N_n values based only on the major magic numbers.

If the β_2 values show certain regularities, so will the $B(E2)$ values. Quite apart from their utility in making predictions of unmeasured $B(E2)$ values through extrapolation or interpolation (the latter being more frequent), these regional trends might have remained somewhat jejune to us had we failed to relate them to some underlying physics.

To understand the regional $B(E2)$ trends, we have invoked three schematic models based on the central idea that the main result of the pp, nn, and pn effective interactions is to give rise to an intrinsic state. This idea implies, in turn, that the $B(E2)$ values are a quadratic function of the linear combination $(e_p N_p + e_n N_n)$ or, more generally, of $(e_p Q_p + e_n Q_n)$. The end result is a family of calculated $B(E2)$ curves when plotted as a function of $N_p N_n$. The spread in these curves can be controlled by choosing an appropriate e_n/e_p ratio, and the agreement between the resulting family of curves and the experimental data is good.

From a purely empirical point of view it should be possible, of course, to force a single curve (or two curves) to approximately represent the $B(E2)$ trend in a particular region. From a theoretical point of view, however, it would be difficult to either explain such a curve or deduce a relationship in which the $B(E2)$ values depend solely or even dominantly on just the $N_p N_n$ product. Thus, while retaining the spirit of earlier conjectures that nuclear deformation should be some dominant function of $N_p N_n$ [and hence $B(E2)$ values at least a quadratic function of $N_p N_n$], the eventual relationships that we have arrived at differ in details and also turn out to be slightly more complex.

ACKNOWLEDGMENTS

We thank P. H. Stelson for contributing his considerable expertise in arriving at the adopted values of Ref. 1. We also thank K. Kumar for making available results of microscopic model calculations and J. B. McGrory for carrying out some single-j calculations. We appreciate the help of R. B. Johnston in preparing the figures. We are indebted to T. Otsuka and G. A. Leander for critically reading the manuscript. One of us (K.B.) is grateful to D. Bryant for facilitating visits to Oak Ridge and to the Oak Ridge National Laboratory for providing kind hospitality. The current research was sponsored by the office of High Energy and Nuclear Physics, U.S. Department of Energy, under Contract No. DE-AC05-84OR21400 with Martin Marietta Energy Systems, Inc.

*On leave of absence from Physical Research Laboratory, Ahmedabad, India 3800015.

[1]S. Raman, C. H. Malarkey, W. T. Milner, C. W. Nestor, Jr., and P. H. Stelson, At. Data Nucl. Data Tables **36**, 1 (1987).

[2]Preliminary results were reported at the American Chemical Society Symposium on Recent Advances in the Study of Nuclei Off the Line of Stability, Chicago, Illinois, 1985; the International Symposium on Weak and Electromagnetic Interactions in Nuclei, Heidelberg, W. Germany, 1986; and the Workshop on Collective Properties of Mid-Mass Nuclei, Tallahassee, Florida, 1987.

[3]L. Grodzins, Phys. Lett. **2**, 88 (1962).

[4]A. Bohr and B. R. Mottelson, Mat. Fys. Medd. Dan. Vid. Selsk. **27**, No. 16 (1953).

[5]C. W. Wang, G. C. Kiang, L. L. Kiang, C. C. Hsu, and E. K. Lin, Chinese J. Phys. **18**, 151 (1980).

[6]C. K. Ross and R. K. Bhaduri, Nucl. Phys. **A196**, 369 (1972).

[7]R. Patnaik, R. Patra, and L. Satpathy, Phys. Rev. C **12**, 2038 (1975).

[8]I. Hamamoto, Nucl. Phys. **73**, 225 (1965).

[9]R. F. Casten, Nucl. Phys. **A443**, 1 (1985).

[10]P. Möller and J. R. Nix, At. Data Nucl. Data Tables **26**, 165 (1981).

[11]R. Bengtsson, P. Möller, J. R. Nix, and Jing-ye Zhang, Phys. Scr. **29**, 402 (1984).

[12]K. Kumar, *Nuclear Models and the Search for Unity in Nuclear Physics* (University of Bergen Press, Bergen, Norway, 1984).

[13]D. J. Rowe, *Nuclear Collective Motion* (Methuen, London, 1970), p. 21.

[14]D. R. Inglis, Phys. Rev. **96**, 1059 (1954).

[15]R. F. Casten, W. Frank, and P. von Brentano, Nucl. Phys. **A444**, 133 (1985).

[16]S. L. Tabor, Phys. Rev. C **34**, 311 (1986).

[17]F. Villars, in *Proceedings of the International School of Physics "Enrico Fermi" Course XXXVI,* edited by C. Bloch (Academic, New York, 1966), p. 14.

[18]M. Harvey, in *Advances in Nuclear Physics,* edited by M. Baranger and E. Vogt (Plenum, New York, 1968), Vol. 1, p. 67.

[19]J. N. Ginocchio and P. Van Isacker, Phys. Rev. C **33**, 365 (1986).

[20]R. F. Casten and A. Wolf, Phys. Rev. C **35**, 1156 (1987).

[21]A. Bohr and B. R. Mottelson, Phys. Scr. **22**, 461 (1980).

[22]T. Otsuka, A. Arima, and F. Iachello, Nucl. Phys. **A309**, 1 (1978).

[23]G. Ripka, in *Advances in Nuclear Physics,* Ref. 18, p. 183.

[24]E. Halbert, J. B. McGrory, and B. H. Wildenthal, Phys. Rev. Lett. **20**, 110 (1968).

[25]K. H. Bhatt, J. C. Parikh, and J. P. Svenne, Phys. Rev. Lett. **21**, 1354 (1968).

[26]A. K. Dhar and K. H. Bhatt, Phys. Rev. C **16**, 792 (1977).

[27]D. P. Ahalpara and K. H. Bhatt, Phys. Rev. C **25**, 2072 (1982).

[28]S. G. Nilsson, Dan. Mat. Fys. Medd. **29**, No. 16 (1955).

[29]An explanation similar to ours has been proffered by Casten, Heyde, and Wolf (private communication) to explain $B(E2)$ saturation in deformed nuclei.

[30]J. H. Hamilton, P. G. Hansen, and E. F. Zganjar, Rep. Prog. Phys. **48**, 631 (1985).

[31]W. Nazarewicz, J. Dudek, R. Bengtsson, T. Bengtsson, and I. Ragnarsson, Nucl. Phys. **A435**, 397 (1985).

[32]D. P. Ahalpara, A. Abzouzi, and K. H. Bhatt, Prog. Part. Nucl. Phys. **15**, 135 (1985).

[33]B. R. Mottelson, in *The Many Body Problem,* edited by C. DeWitt (Wiley, New York, 1959), p. 289.

[34]A. Bohr and B. R. Mottelson, *Nuclear Structure, Vol. II* (Benjamin, Reading, 1975), p. 515.

[35]K. Kumar, in *Structure of Medium Heavy Nuclei 1979,* IOP Conference Series No. 49 (Institute of Physics, Bristol, 1980), p. 169.

[36]K. Kumar, in *Proceedings First International Spring Seminar on Nuclear Physics: Microscopic Approaches to Nuclear Structure Calculations,* Sorrento, Italy, 1986 (Tipografia Compositiori, Bologna, in press).

[37]A. Subber, W. D. Hamilton, P. Park, and K. Kumar, J. Phys. G **13**, 161 (1987).

[38]A. R. H. Subber, S. J. Robinson, P. Hungerford, W. D. Hamilton, P. Van Isacker, K. Kumar, P. Park, K. Schreckenbach, and G. G. Colvin, J. Phys. G (to be published).

[39]S. A. Hamada, W. D. Hamilton, and K. Kumar, private communication.

[40]S. Eid, J. Copnell, W. D. Hamilton, and K. Kumar, private communication.

[41]D. Vautherin, Phys. Rev. C **7**, 296 (1973).